Binocular Imaging of a Laser Stripe and Approximation Networks for Shape Detection

J. Apolinar Muñoz-Rodríguez

Centro de Investigaciones en Optica, A. C., Leon, Gto, 37150 Mexico

Received 28 August 2006; accepted 11 June 2007

ABSTRACT: A technique for shape detection based on binocular imaging of a laser stripe is presented. In this technique, the object shape is recovered by means of laser stripe projection and binocular imaging. The approach of the binocular imaging in this technique is to avoid stripe occlusions, which appear due to the variation to the object surface. Based on the behavior of the stripe displacement, the object topography is computed by a Bezier approximation network. By means of this network, the measurements of the binocular geometry are avoided. The parameters of the binocular imaging are computed based on the Bezier approximation network. To reconstruct the topography, the object is scanned by a laser stripe. From the scanning, a set of binocular images of the stripe are processed to compute the object dimensions by means of the network. By applying Bezier approximation networks, the performance of the binocular imaging and the accuracy are improved. It is because the errors of the measurement are not added to the computational procedure, which performs the shape reconstruction. This procedure represents a contribution for the stripe projection methods and the binocular imaging. To describe the accuracy a root mean square of error is calculated. This technique is tested with real objects and its experimental results are presented. Also, the time processing is described. Int J Imaging Syst Technol, 17, 62–74, 2007; Published online in Wiley InterScience (www.interscience.wiley.com). DOI 10.1002/ima.20099

Key words: binocular imaging; laser stripe; Bezier approximation networks

I. INTRODUCTION

In optical metrology and robotics vision, optical systems have been applied for shape detection. The use of structured light makes the system more reliable and the acquired data are easier to interpret. A particular technique is the laser stripe projection (Mclor, 2002; Wei et al., 2003; Zagorchev and Goshtasby, 2006). When a stripe is projected on an object, the stripe is moved in the image due to the surface variation. It is because the viewer is placed at a different direction from the stripe projection. From the stripe position in the image and the geometry of the setup, the object contour is computed. In this technique, the main aim is the detection of the stripe position in the image (Tai and Chang, 1996; Baba et al., 1998; Muñoz Rodríguez and Rodríguez-Vera, 2003). Also, the geometry of the setup is measured to obtain the object topography. Some times, an area of the stripe is occluded due to the surface variation. When it happens, the stripe cannot be detected in the occluded region. Therefore, the stripe occlusion causes a problem to retrieve the object shape (Luo et al., 2003; Mitsudo, 2006).

In the proposed technique here, the object shape is detected by stripe projection and the occluded areas are detected by binocular imaging. To perform the contouring, the object is scanned by a laser stripe. In this procedure, a pair of binocular images of the stripe is captured. Based on the behavior of the stripe position at the image, the object contour is retrieved. When the surface variation produces an occlusion, the occluded stripe appears in only one of the two images. In this case, the stripe occlusion in the first image is not occluded in the second image. Also, the stripe occlusion of the second image is not occluded in the first image. Thus, the object contour missed in each image can be retrieved from each other. In this manner, the stripe occlusion is avoided by the binocular imaging.

For a binocular system, the focal length, the distance between two cameras, and the disparity are needed to perform the object contouring (Andersen et al., 2005). The disparity is the entity that provides the object contour. This is because the other parameters are constants. The disparity is deduced by the two distances, from the image center to the pattern position of the binocular images. In the proposed technique, only one distance of the disparity is used to compute the object depth. This means that only the stripe position of one camera is needed to perform the contouring. Thus, the object depth is computed based on the pattern position of the disparity. To carry it out, a Bezier approximation network (BAN) generates a function that describes object depth according to the stripe position. The architecture of the BAN is constructed using the position of stripe projected on objects with known dimensions. Thus, the BAN performs the contouring based on the stripe position. In this manner, the contouring is performed automatically by computational algorithms. Also, the focal length, the distance between the two cameras, image center, camera orientation, and pixel dimensions are computed based on the BAN and image processing. Thus, the physical measurements on the setup are avoided. This kind of computational process provides a better performance and accuracy. This

Correspondence to: J. Apolinar Muñoz-Rodríguez; e-mail: munoza@foton.cio.mx

procedure represents a contribution for the stripe projection methods and in the binocular imaging methods.

In the contouring procedure, the object is moved in the x-axis and a set of binocular images of the stripe is captured. Each one of these images is processed to detect the position of the stripe disparity. This stripe position is processed by the BAN to determine the object contour. The produced information by the binocular images of the stripe corresponds to a transverse section of the object. The data of the transverse sections are stored in an array memory to obtain the complete object shape. The technique is tested with plastic objects, ceramic objects, and metallic objects and the results are achieved with good repeatability.

II. DESCRIPTION OF THE OPTICAL SETUP

The proposed setup Figure 1 consists of a stripe projector, two CCD cameras, an electromechanical device, and a computer. In this arrangement, the object is fixed on a platform of the electromechanical device. By means of a stepping motor, the platform moves the object in the x-axis with an accuracy of a fraction of millimeter. To perform the scanning, a laser stripe is projected onto the object surface by a laser diode. In each step of the scanning, the laser stripe is digitized by two CCD cameras and a frame grabber. In each binocular image, the stripe is deformed in the x-axis according to the object surface. The profilometric method is based on the displacement of the stripe deformation. By detecting the position of the stripe displacement, the object contour is determined. In this manner, the stripe position is main parameter to perform the object contouring. Therefore, stripe occlusions should be avoided. When an occlusion appears, the object contour is not completed. To retrieve the complete object contour, the binocular imaging is applied. In this system, the stripe occluded in the first camera can be observed by the second camera. Also, the stripe occluded the second camera can be observed by the first camera. Thus, the binocular system overcomes the occlusion problem in the stripe projection. In this manner, the object contour can be computed completely.

The contouring method is described based on the geometry shown in Figure 2. On the reference plane are located the x-axis, y-axis, and the object depth is indicated by $h(x, y)$ in the z-axis. The points o and p correspond to stripe projected on the reference plane and object surface, respectively. The focal length is indicated by F, d is the distance between the two cameras and the image center of each camera is indicated by ax_c and ex_c, respectively. When a laser stripe is projected on the target, the stripe position is moved from ax_o to ax_p in the image plane of the camera a. At the same time, the stripe position is moved from ex_o to ex_p in the camera e. The stripe displacement in the image plane for each camera is represented by

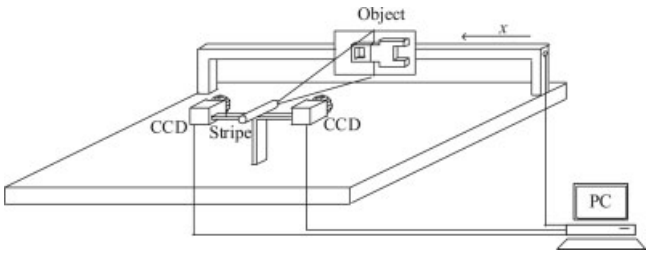

Figure 1. Experimental setup.

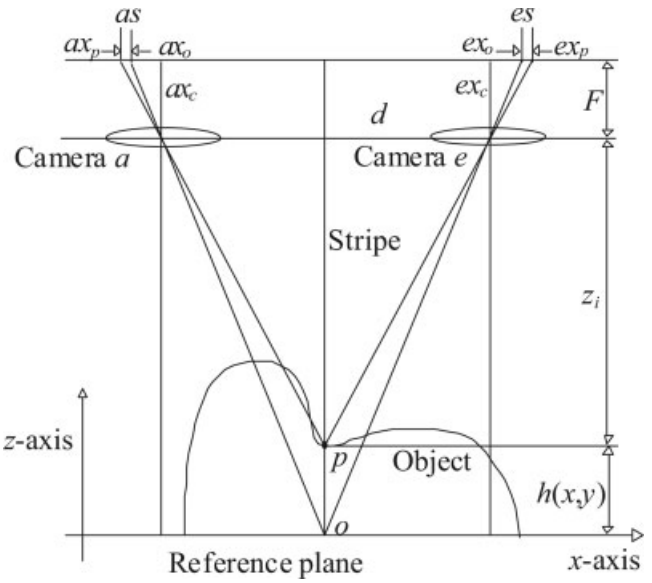

Figure 2. Geometry of the experimental setup.

$$as(x, y) = ax_o - ax_p \tag{1}$$

$$es(x, y) = ex_p - ex_o \tag{2}$$

By means of the positions ex_p and ax_p, the stripe displacement respect to the reference point "o" is given by $as(x,y)$ for the camera a and $es(x,y)$ for the camera e. Based on the pinhole camera model (Klette, 1998), the surface z_i in a binocular system is deduced by

$$z_i = \frac{dF}{\delta + \varepsilon}, \tag{3}$$

from this equation, $\delta + \varepsilon$ is the disparity. The distances of the disparity are deduced by $\delta = ax_c - ax_p$ and $\varepsilon = ex_c - ex_p$, respectively. To compute the surface z_i by means of Eq. (3), the constants F, d, ax_c, ex_c and camera orientation should be known. In each camera the surface z_i is computed by

$$z_i = \frac{F \cdot \ell a}{\delta}, \tag{4}$$

$$z_i = \frac{F \cdot \ell e}{\varepsilon} \tag{5}$$

Where Eq. (4) corresponds to camera a, Eq. (5) corresponds to the camera e and $a + \ell e = d$. In the stripe projection technique, the camera orientation, F, ℓa or ℓe are obtained by an external procedure to the contouring. Then, these parameters are given to the computer to reconstruct the object shape. This means that Eq. (3), Eq. (4) or Eq. (5) can not be computed in the procedure of contouring by pattern position from image processing.

For the proposed technique, the object depth $h(x,y)$ is computed directly in the image processing of pattern position. In this procedure, a BAN provides a function that computes the object dimension based on the stripe displacement. Also, this network provides information of the camera orientation, the focal lens, the center coordinates, the distance between tow cameras, disparity and center

coordinates. Thus, the performance for object contouring is improved. The procedure to determine the camera parameters is described in section V. In the proposed technique, the object depth is computed by the BAN based on the stripe position using only one camera of the binocular system. The network produces the object dimension $h(x,y)$ using $as(x,y)$ or $es(x,y)$. The image processing provides a least one of the two stripe displacements. When a stripe occlusion appears in the image of camera a, $as(x,y)$ is missing. Then, the ex_p of the stripe disparity is used to produce the object depth $h(x,y)$. Thus, the binocular imaging system provides the stripe displacement. In this manner, the occlusion problem of the stripe is solved by the binocular imaging. To detect the disparity, the stripe position is measured in every row of the binocular images. This position is computed by detecting the maximum position of the stripe intensity in each row of the image. Then, the stripe position is processed by the BAN to perform the object contouring. With all images, the complete object shape is reconstructed. In section III, the image processing of a stripe is described.

III. IMAGE PROCESSING OF A STRIPE

The intensity projected by a laser diode is a Gaussian distribution in the x-axis (Causa and Sarma, 2003). The intensity in every row of the image is represented by (x_0, z_0), (x_1, z_1), (x_2, z_2), ... ,(x_n, z_n), where x_i is the pixel position and z_i is the pixel intensity. To detect the stripe position, the maximum intensity measured in the image. To carry it out, Gaussian approximation and peak detection are used. A simple manner to detect the stripe position is the Gaussian function, which is described by

$$f(x) = \frac{Ni}{\sigma\sqrt{2\pi}} e^{-\frac{1}{2}\left(\frac{x-\mu}{\sigma}\right)^2}, \tag{6}$$

where Ni is the area under the curve, μ is the mean of the function, and σ is the standard deviation (Milton and Arnold, 2003). In this case, μ represents the position of the maximum of the Gaussian function. Therefore, the stripe position is detected by computing the mean μ in every row of the image by

$$\mu = \frac{\sum_{i=1}^{n} z_i x_i}{\sum_{i=1}^{n} z_i}, \tag{7}$$

Figure 3 shows pixels of a row of a stripe image. To determine the stripe position from these pixels, the mean μ is computed substituting the position x_i and the intensity z_i into Eq. (7). In this case the result is μ = 14.664. Therefore, the stripe position is ax_P = 14.664 pixels. Also, the factor of normalization and the standard deviation are calculated to fit the Gaussian function shown in Figure 3. Usually μ is calculated using the arithmetic mean, which provides the middle point of the pixels. The result of the arithmetic mean of Figure 3 is μ = 14.5 pixels. However, the maximum is at left hand or right hand of the middle point due to the camera position. The Eq. (7) is called weighted arithmetic mean (Milton and Arnold, 2003), which assigns a weight to every point. In this case the weight is the pixel intensity. It means that a pixel of major intensity is more important than a pixel of low intensity. Also, the Least squared method (Gerald and Wheatley, 1992) can be used to detect the maximum position. To carry it out, the pixels of Figure 3 are adjusted to a third equation by

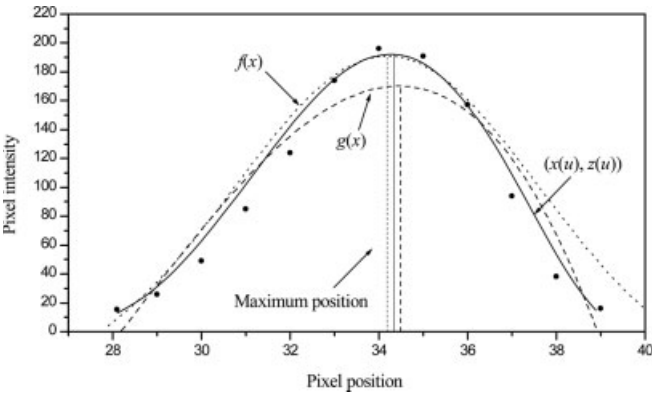

Figure 3. Maximum position from a set of pixels fitted to a Gaussian function, Least square method and Bezier curves.

$$g(x) = \mu_0 + \mu_1 x + \mu_2 x^2 + \mu_3 x^3, \tag{8}$$

where $g(x)$ represents the stripe intensity in the x-axis and μ_0, μ_1, μ_2, μ_3, are the constants for a particular curve. The Least squared criterion indicates that

$$S = \sum_{i=0}^{n} (z_i - \mu_0 - \mu_1 x_i - \mu_2 x_i^2 - \mu_3 x_i^3)^2, \tag{9}$$

be a minimum. At minimum for S the partial derivatives will be zero:

$$\frac{\partial S}{\partial \mu_0} = 0, \quad \frac{\partial S}{\partial \mu_1} = 0, \quad \frac{\partial S}{\partial \mu_2} = 0, \quad \frac{\partial S}{\partial \mu_3} = 0.$$

Expanding the summation of these derivatives, an equations system is obtained. By solving this system, the constants μ_0, μ_1, μ_2, μ_3, are determined. These constants are substituted into Eq. (8) to fit the curve shown in Figure 3 by dash line. Then, the first and the second derivative are applied to determine the local maximum or minimum. In this case, the second derivative is greater than zero ($g''(x) > 0$) in the interval from x_0 to x_n (Frederick and Lieberman, 1982). Thus, the maximum position is obtained by the first derivative where $g'(x) = 0$. To find the value x^* for $g'(x) = 0$, the Bisection method is used (Gerald and Wheatley, 1992). Beginning with values $x_i = x_0$ and $x_s = x_n$, and x^* is half point between x_i and x_s. If $g'(x)$ evaluated at $x = x^*$ is positive, then $x_i = x^*$. If $f'(x)$ evaluated at $x = x^*$ is negative, then $x_s = x^*$. Next x^* is taken as the mid point of the last pair of values that converges to the root. For the curve of Figure 3 the result is $x^* = 34.456$ and the stripe position is $ax_p = 34.456$ pixels.

Also, Bezier Curves are used to detect the stripe position. The nth-degree Bezier function is determined by n + 1pixels (Gasson, 1989). The nth-degree Bezier function is determined by two parametric equations, which are described by

$$x(u) = \binom{n}{0}(1-u)^n u^0 x_0 + \binom{n}{1}(1-u)^{n-1} u x_1 + \cdots\cdots + \binom{n}{n}(1-u)^0 u^n x_n, \quad 0 \le u \le 1. \tag{10}$$

$$z(u) = \binom{n}{0}(1-u)^n u^0 z_0 + \binom{n}{1}(1-u)^{n-1} u z_1 + \cdots\cdots + \binom{n}{n}(1-u)^0 u^n z_n, \quad 0 \le u \le 1. \tag{11}$$

Eq. (10) represents the pixel position and Eq. (11) represents the pixel intensity. To fit the Bezier curve shown in Figure 3, x_0, x_1,

Figure 4. (a) First stripe captured by the binocular system. (b) Second stripe captured by the binocular system.

$x_2, \ldots, x_n$, are substituted into Eq. (10) and $z_0, z_1, z_2, \ldots, z_n$, are substituted into Eq. (11). Then, these equations are evaluated in the interval $0 \leq u \leq 1$. In this case, the second derivative $z''(u) > 0$ in the interval $0 \leq u \leq 1$. Therefore, the maximum is detected by the first derivative equal to zero $z'(u) = 0$ via bisection method. Beginning with a pair of values $u_i = 0$ and $u_s = 1$, because $z(u)$ is defined for the interval $0 \leq u \leq 1$, u^* is halfway between u_i and u_s. If $z'(u)$ evaluated at $u = u^*$ is positive, then $u_i = u^*$. If $z'(u)$ evaluated at $u = u^*$ is negative, then $u_s = u^*$. Next, u^* is taken as the mid point of the last pair values that converges to the root. The value u^* where $z'(u) = 0$ is substituted into Eq. (11) to obtain maximum position x^*. The result is $x^* = 34.274$ and the stripe position is $ax_p = 34.274$ pixels, which is shown in Figure 3.

The examination of these three methods is based on the best accuracy provided by the stripe detection. According to the root mean square of error (rms), the stripe detection by Bezier curves provides the best accuracy. The results of this examination are presented in section VI. The procedure of stripe detection is applied to all rows of the image to obtain a contour. This procedure is applied to the binocular images shown in Figures 4a and 4b, respectively. From these images, the stripe position ax_p and ex_p are computed along the y-axis. Then, the displacement $as(x,y)$ and $es(x,y)$ are computed via Eq. (1) and Eq. (2), respectively. These stripe displacements are shown Figures 5a and 5b, respectively. The contour of Figure 5a is not completed due to the occlusion in Figure 4a. But, Figure 4b does not contain stripe occlusions and the complete contour is achieved in Figure 5b. The binocular images Figures 4a and 4b correspond to a stripe projected on a dummy face. The intensity reflected by the object surface is very similar to intensity reflected by the reference plane. The powerful of the stripe detection is elucidated in surfaces without uniform reflection. To carry it out, a stripe projected on plastic Figure 6a, metallic Figure 6b and ceramic surface Figure 6c are processed. The reflected intensity by the ceramic surface is similar to the intensity reflected by the reference plane. The reflected intensity by the metallic surface and plastic surface are different to the intensity reflected by the reference plane. The stripe intensity reflected by these surfaces is not so good. However, Bezier curves produced a smooth intensity from the reflected stripe.

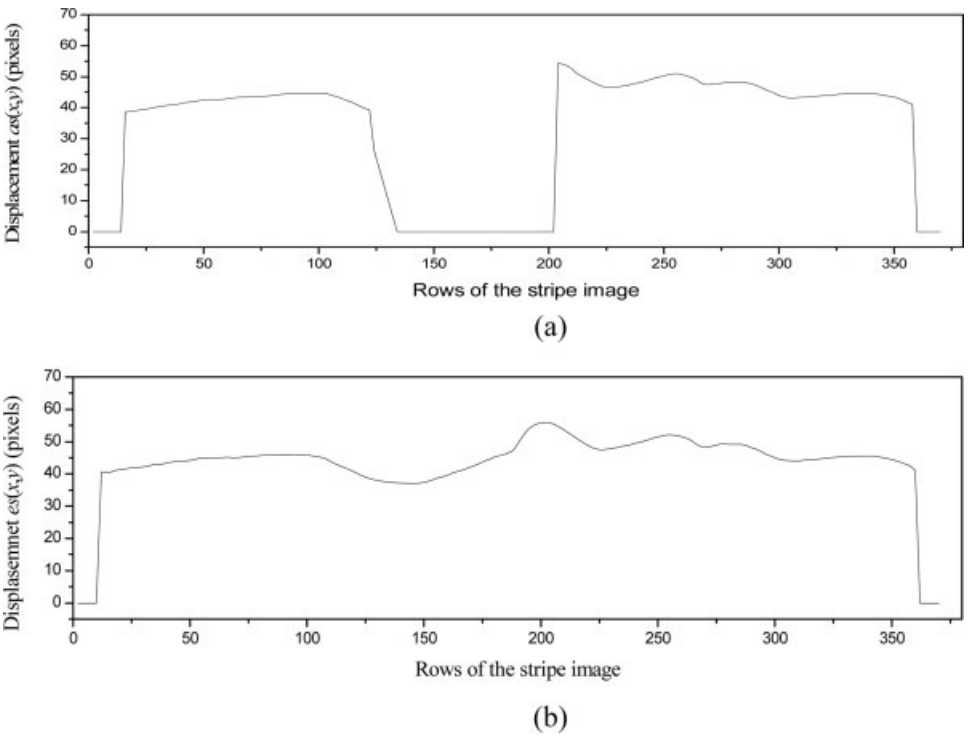

Figure 5. (a) Stripe displacement $as(x,y)$ obtained from Figure 4a. (b) Stripe displacement $es(x,y)$ obtained from Figure 4b.

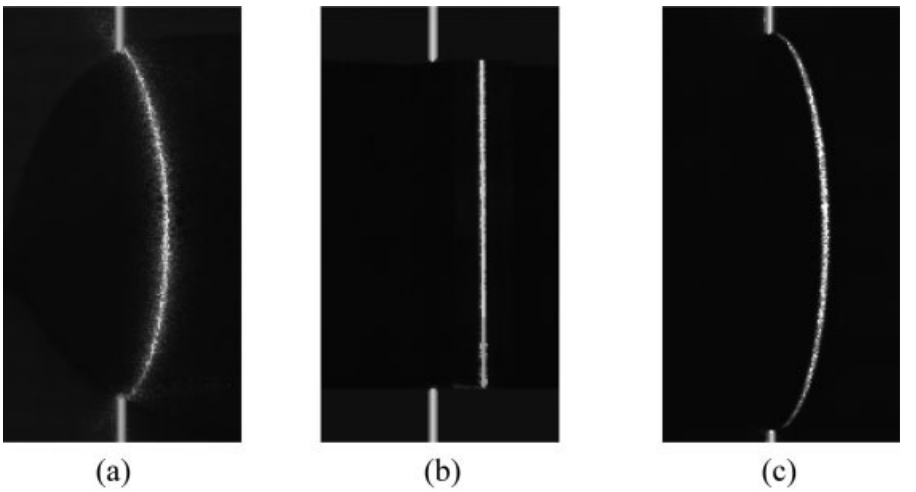

Figure 6. (a) Stripe projected on plastic surface. (b) Stripe projected on metallic surface. (c) Stripe projected on ceramic surface.

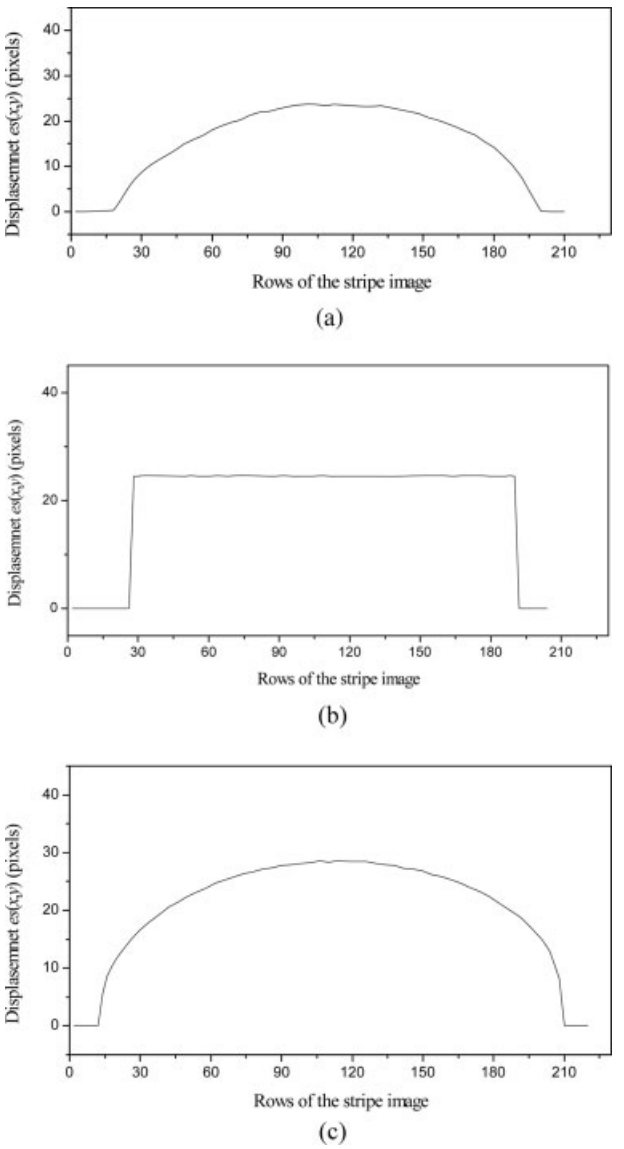

Figure 7. (a) Stripe displacement obtained from Figure 6a. (b) Stripe displacement obtained from Figure 6b. (c) Stripe displacement obtained from Figure 6c.

Thus, displacement is computed in good manner as is shown in Figures 7a, 7b, 7c, respectively. The object shape of these objects is shown in section VI.

IV. STRUCTURE OF BANS

From the Binocular images, the stripe displacement is proportional to the object dimension. A BAN is built to compute the object dimension $h(x,y)$ by means of the stripe displacement $as(x,y)$ or $es(x,y)$. This network is constructed based on a stripe projected on objects with known dimensions. The BAN structure Figure 8

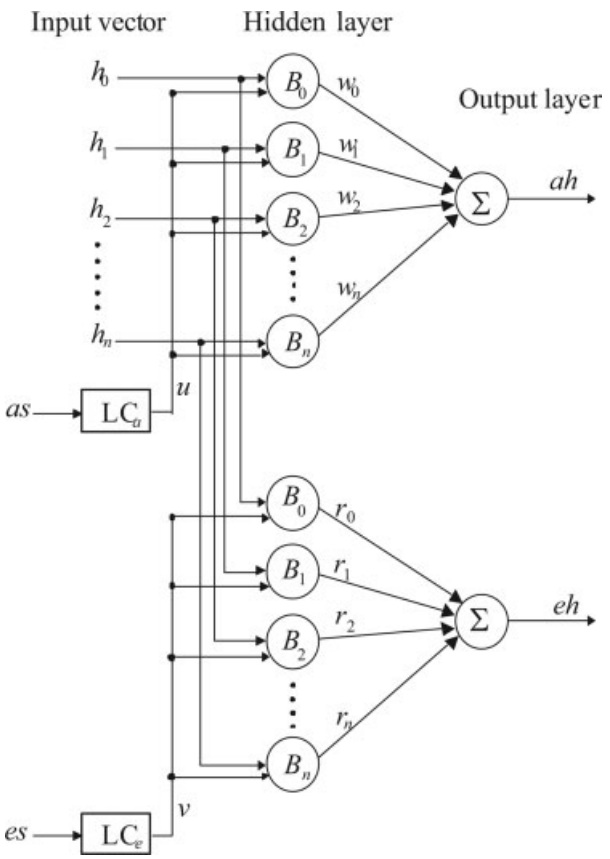

Figure 8. Structure of the BAN proposed in this technique.

consists of an input vector, a parametric input, a hidden layer and an output layer. Each layer of the network is deduced as follow. The input includes: the object dimensions h_i, the stripe displacements *as*, *es* and the parametric values u and v. The input data as_0, as_1, $as_2, \ldots, as_n$ and es_0, es_1, $es_2, \ldots, es_n$ are the stripe displacements obtained by image processing described in section II. By means of these displacements, a linear combination LC_a and LC_e are determined (Schalkoff, 1997) to compute u and v. The relationship between the displacement and the parametric values is described by

$$u = b_0 + b_{1as}, \tag{12}$$

$$v = c_0 + c_{1es}, \tag{13}$$

where b_i and c_i are the unknown constants. The Bezier curves are defined in the interval $0 \leq u \leq 1$ and $0 \leq v \leq 1$ (Ahn et al., 2004). For the dimension h_0, the displacements as_0 and es_0 are produced. Therefore, $u = 0$ for as_0 and $v = 0$ for es_0. For h_n the displacements as_n and es_n are produced. Therefore, the $u = 1$ for as_n and $v = 1$ for es_n is. Substituting the values (as_0, $u = 0$) and (as_n, $u = 1$) in Eq. (12), two equations with two unknown constants are obtained. Solving these equations b_0 and b_1 can be determined. In this manner, Eq. (12) is completed. Substituting the values (es_0, $v = 0$) and (es_n, $v = 1$) in Eq. (13), two equations with two unknown constants are obtained. Solving these equations c_0 and c_1 are determined. In this manner, Eq. (13) is completed. Thus, for the displacement *as* and *es*, the parametric values u and v are computed via Eq. (12) and Eq. (13), respectively. The input h_0, h_1, $h_2, \ldots, h_n$ are obtained from the pattern objects, whose dimensions are known. The hidden layer is constructed by Bezier basis function (Chen and Wang, 2002), which is described by

$$B_i(u) = \binom{n}{i} u^i (1-u)^{n-i}, \quad \text{and} \quad \binom{n}{i} = \frac{n!}{i!(n-i)!}, \tag{14}$$

denotes the binomial distribution from statistics. The output layer is the summation of the neurons of the hidden layer, which are multiplied by a weight. The output is the dimension $h(x,y)$, which is represented by $ah(u)$ and $eh(v)$. These two outputs are described by the next equations

$$ah(u) = \sum_{i=0}^{n} w_i B_i(u) h_i, \quad 0 \leq u \leq 1, \tag{15}$$

$$eh(v) = \sum_{i=0}^{n} r_i B_i(v) h_i, \quad 0 \leq v \leq 1, \tag{16}$$

where w_i and r_i are the weights, h_i is the known dimension of the pattern objects and B_i is the Bezier basis function Eq. (14). To obtain the BAN Eq. (15) and Eq. (16), the suitable weights w_i and r_i should be determined. To obtain the weights w_0, w_1, $w_2, \ldots, w_n$, the network is being forced to produce the outputs h_0, h_1, $h_2, \ldots, h_n$ by means of an adjustment mechanism (Gasson, 1989). To carry it out, the values h_i and its u are substituted in Eq. (15). The value u is computed via Eq. (12) based on the displacement *as*, which corresponds to the known dimension h_i. For each input u, an output *ah* is produced. Thus, the next equation system is obtained

$$\begin{aligned}
ah_0 = h_0 &= w_0 \binom{n}{0}(1-u)^n u^0 h_0 + w_1 \binom{n}{1}(1-u)^{n-1} u h_1 + \cdots\cdots + w_n \binom{n}{n}(1-u)^0 u^n h_n, \quad 0 \leq u \leq 1. \\
ah_1 = h_1 &= w_0 \binom{n}{0}(1-u)^n u^0 h_0 + w_1 \binom{n}{1}(1-u)^{n-1} u h_1 + \cdots\cdots + w_n \binom{n}{n}(1-u)^0 u^n h_n, \quad 0 \leq u \leq 1. \\
&\vdots \qquad\qquad \vdots \qquad\qquad \vdots \qquad\qquad\qquad \vdots \\
ah_n = h_n &= w_0 \binom{n}{0}(1-u)^n u^0 h_0 + w_1 \binom{n}{1}(1-u)^{n-1} u h_1 + \cdots\cdots + w_n \binom{n}{n}(1-u)^0 u^n h_n, \quad 0 \leq u \leq 1.
\end{aligned} \tag{17}$$

This linear system of Eq. (17) can be represented as

$$\begin{aligned}
h_0 &= w_0\beta_{0,0} + w_1\beta_{0,1} + \cdots\cdots\cdots + w_n\beta_{0,n} \\
h_1 &= w_0\beta_{1,0} + w_1\beta_{1,1} + \cdots\cdots\cdots + w_n\beta_{1,n} \\
&\vdots \qquad \vdots \qquad \vdots \qquad\qquad\qquad \vdots \\
h_n &= w_0\beta_{n,0} + w_1\beta_{n,1} + \cdots\cdots\cdots + w_n\beta_{n,n}
\end{aligned} \tag{18}$$

This equation can be rewritten as the product between the matrix of the input data and the matrix of the corresponding output values: $\boldsymbol{\beta}\mathbf{W} = \mathbf{H}$. The linear system represented by the next matrix

$$\begin{bmatrix} \beta_{0,0} & \beta_{0,1} & \beta_{0,2} & \cdots & \beta_{0,n} \\ \beta_{101} & \beta_{1,1} & \beta_{1,2} & \cdots & \beta_{1,n} \\ \vdots & \vdots & \vdots & & \vdots \\ \beta_{n,0} & \beta_{n,1} & \beta_{n,2} & \cdots & \beta_{n,n} \end{bmatrix} \begin{bmatrix} w_0 \\ w_1 \\ \vdots \\ w_n \end{bmatrix} = \begin{bmatrix} h_0 \\ h_1 \\ \vdots \\ h_n \end{bmatrix} \tag{19}$$

This system Eq. (19) is solved by the Chelosky method (Press, 1993). Thus the weights w_0, w_1, $w_2, \ldots, w_n$ are calculated. In this manner, Eq. (15) has been completed.

To determine the weights r_0, r_1, $r_2, \ldots, r_n$, again, the network is being forced to produce the outputs h_0, h_1, $h_2, \ldots, h_n$. r_i. To carry it out, the values v and h_i are substituted in Eq. (16). The value v is calculated via Eq. (13) using the displacement *es*, which corresponds to the dimension h_i. For each input v, an output *eh* is produced and the next equation system is obtained

$$
\begin{aligned}
eh_0 = h_0 &= r_0\binom{n}{0}(1-v)^n v^0 h_0 + r_1\binom{n}{1}(1-v)^{n-1} v h_1 + \cdots + r_n\binom{n}{n}(1-v)^0 v^n h_n, \quad 0 \le v \le 1.\\
eh_1 = h_1 &= r_0\binom{n}{0}(1-v)^n v^0 h_0 + r_1\binom{n}{1}(1-v)^{n-1} v h_1 + \cdots +, + r_n\binom{n}{n}(1-v)^0 v^n h_n, \quad 0 \le v \le 1.\\
&\vdots \qquad\qquad \vdots \qquad\qquad \vdots \qquad\qquad \vdots\\
eh_n = h_n &= r_0\binom{n}{0}(1-v)^n v^0 h_0 + r_1\binom{n}{1}(1-v)^{n-1} v h_1 + \cdots +, + r_n\binom{n}{n}(1-v)^0 v^n h_n, \quad 0 \le v \le 1.
\end{aligned}
\tag{20}
$$

The linear system Eq. (20) can be represented as the product between the input matrix and the matrix of the corresponding output: $\Im\,\mathbf{R} = \mathbf{H}$. The linear system represented by the next matrix

$$
\begin{bmatrix}
\Im_{0,0} & \Im_{0,1} & \Im_{0,2} & \cdots & \Im_{0,n}\\
\Im_{101} & \Im_{1,1} & \Im_{1,2} & \cdots & \Im_{1,n}\\
\vdots & \vdots & \vdots & & \vdots\\
\Im_{n,0} & \Im_{n,1} & \Im_{n,2} & \cdots & \Im_{n,n}
\end{bmatrix}
\begin{bmatrix} r_0\\ r_1\\ \vdots\\ r_n \end{bmatrix}
=
\begin{bmatrix} h_0\\ h_1\\ \vdots\\ h_n \end{bmatrix}
\tag{21}
$$

This linear system Eq.(21) is solved by the Chelosky and the weights $r_0, r_1, r_2, \ldots, r_n$ are determined. In this manner, Eq. (16) has been completed. Thus, the BAN produces the shape dimension via Eq. (16) and Eq. (17) based on the stripe displacement *as* and *es,* respectively. In this manner, the BAN provides the object depth by means of $h(x,y) = ah(u)$ and $h(x,y) = eh(v)$.

V. PARAMETERS OF THE IMAGING SYSTEM

In optical metrology, the object shape is reconstructed based on the parameters of the camera and the setup. Usually, these parameters are computed by external procedure to the reconstruction system. Then, the object shape is determined based on these parameters. The camera parameters include focal distance, image center coordinates, pixel dimension, distortion and camera orientation. In the proposed binocular system, the camera parameters are determined in the reconstruction system by the BAN and image processing. The camera parameters are determined based on the pinhole camera model, which is shown in Figure 9. In the binocular system, the optical axis of the cameras is perpendicular to the reference plane. The camera orientation in the *x*-axis is determined by means of the geometry Figure 10a. In this geometry, the stripe projected on the reference plane and the object is indicated by ax_o and ax_p at the image plane, respectively. The distance between the image center and the laser stripe in the *x*-axis is indicated by ℓ_a. The object dimension is indicated by h_i and $D = z_i + h_i$. In this case, the reference plane is a platform, which can be moved in the *x*-axis. For this geometry, the camera orientation is performed by s_i and h_i of the BAN. According to the perpendicular optical axis, the object depth h_i has a projection k_i in the reference plane. From Figure 10a, the displacement is defined as $s_i = (ax_c - ax_p) - (ax_c - ax_o)$. Thus, the projection k_i at the reference plane is computed by

$$
k_i = \frac{Fh_i}{s_i + ax_c - ax_o} \tag{22}
$$

From Eq. (22) F, ax_c, ax_o are constants and h_i is computed by the BAN according to s_i. In this case, k_i is a linear function. Therefore, the derivative k_i respect to s_i dk/ds is a constant. Other configuration is an optical axis not perpendicular to the reference plane, which is shown in Figure 10b. For this geometry, the component δ is defined by $ax_c - ax_p = F \tan\theta$ and the displacement is defined by $s_i = F \tan\theta - (ax_c - ax_o)$. The angles of this geometry are defined by $\theta + \beta + \alpha = 180$, $\alpha + \gamma = 90$, and $k_i = h_i \tan\gamma$. Therefore, projection is given by

$$
k_i = h_i \tan\left[\tan^{-1}\left(\frac{s_i + ax_c - ax_o}{F}\right) + \beta - 90^\circ\right] \tag{23}
$$

From Eq. (23) F, ax_c, ax_o, and β are constants and h_i is computed by $h_i = D - \ell_a \tan\alpha$. Where β is an angle minor than 90° and D is constant. In this case, s_i does not produce a linear function k_i in Eq. (23). Also, the derivative dk/ds is not a constant.

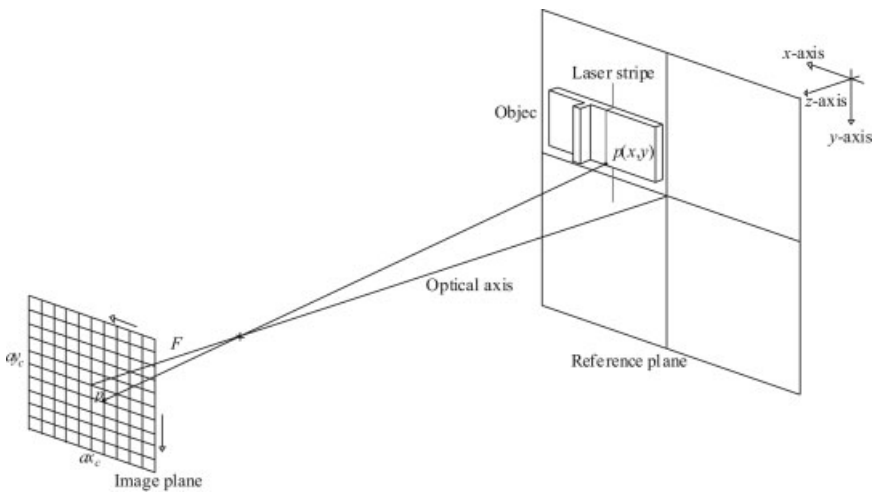

Figure 9. Geometry of the pinhole camera model.

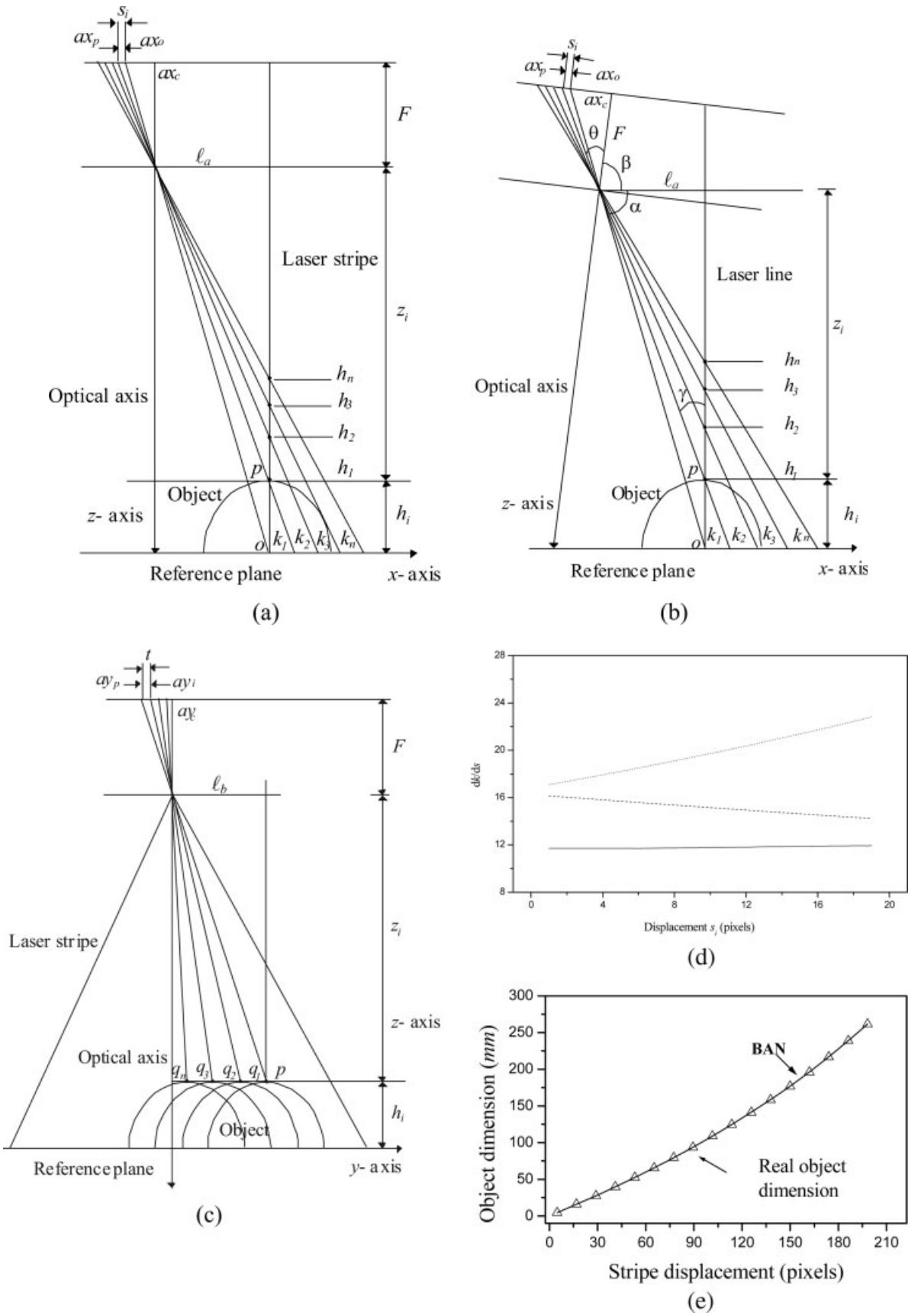

Figure 10. (a) Geometry of an optical axis perpendicular to *x*-axis. (b) Geometry of an optical axis not perpendicular to *x*-axis. (c) Geometry of an optical axis perpendicular to *y*-axis. (d) Derivative *dk*/*ds* for an optical axis perpendicular to *x*-axis and for an optical axis not perpendicular to *x*-axis. (e) Function produced by the BAN, which provides the object dimension.

The orientation of the camera in y-axis is performed based on the geometry of Figure 10c. In this case, the object is moved in y-axis over the laser stripe. When the object is moved, the pattern position changes from ay_p to ay_i in the laser stripe. In this case, $t = (ay_c - ay_p) - (ay_c - ay_i)$. For an optical axis perpendicular to the reference plane y-axis, a linear q produces a linear t at the image plane. Therefore, the derivative dt/dq is a constant. Thus, the orientation camera is performed by means of dk/ds = constant for the x-axis and dt/dq = constant for the y-axis.

Based on these criterions, the optical axis is aligned perpendicular to x-axis and y-axis. For the orientation in x-axis, k_i is computed from h_i provided by the BAN. Because of the distortion, the derivative dk/ds is slightly different to a constant. But, this derivative is the more similar to a constant, which is shown in Figure 10d. In this figure, the dash line is dk/ds for β minor than 90° and the dot line is dk/ds for β major than 90°. Thus, the generated BAN corresponds to an optical axis aligned perpendicularly to the x-axis. For the orientation in y-axis, q_i is provided by the electromechanical device and t is obtained by image processing. In this process, the object position is detected in the stripe in each movement. Because of the distortion, the derivative dt/dq is not exactly a constant. But, this derivative is the more similar to a constant. Thus, the optical axis is aligned perpendicular to the y-axis. In this manner, the BAN and image processing provide an optical axis aligned perpendicularly to the reference plane.

Based on the optical axis perpendicular to reference plane Figure 10a, the camera parameters are obtained. To carry it out, the BAN produces the object depth h_i based on s_i for the calibration. The geometry of the setup Figure 10a is described by

$$\frac{z_i}{\ell_a} = \frac{z_i + F}{\eta(ax_c - ax_p) + \ell_a}, \tag{24}$$

From this equation η is scale factor to convert the pixels to millimeters. Using $D = z_i + h_i$ and $\eta s_i = \eta\ (ax_c - ax_p) - \eta\ (ax_c - ax_o)$, Eq. (24) is rewritten as

$$\frac{D - h_i}{\ell_a} = \frac{D - h_i + F}{\eta(s_i + ax_c - ax_o) + \ell_a} \tag{25}$$

Where D is the distance from the lens to the reference plane. From Eq. (25) the constants D, ℓ_a, F, η, ax_c and ax_o should be determined. To carry it out, Eq. (25) is rewritten as equation system

$$\begin{aligned}
h_1 &= D - \frac{F\ell_a}{\eta(s_1 + ax_c - ax_o)} \\
h_2 &= D - \frac{F\ell_a}{\eta(s_2 + ax_c - ax_o)} \\
h_3 &= D - \frac{F\ell_a}{\eta(s_3 + ax_c - ax_o)} \\
h_4 &= D - \frac{F\ell_a}{\eta(s_4 + ax_c - ax_o)} \\
h_5 &= D - \frac{F\ell_a}{\eta(s_5 + ax_c - ax_o)} \\
h_6 &= D - \frac{F\ell_a}{\eta(s_6 + ax_c - ax_o)}
\end{aligned} \tag{26}$$

The values $h_1, h_2, \ldots, h_6$, are computed by the BAN according to $s_1, s_2, \ldots, s_6$. These values are substituted in Eq. (26) and the equation system is solved. Thus, the constants D, ℓ_a, F, η, ax_c, and ax_o are determined. The coordinate ay_c is computed from the geometry Figure 10c described by

$$t_i = (ay_c - ay_p) - \frac{F(D - h_i)}{\eta(\ell_b - q_{i-1})}, \tag{27}$$

From Eq. (27) the constants D, F, η, q_i, t_i, h_i are known and ay_c, ℓ_b, ay_p should be determined. To carry it out, Eq. (27) is rewritten as equation system for an h_i constant by

$$\begin{aligned}
t_1 &= (ay_c - ay_p) - \frac{F(D - h_1)}{\eta(g - q_0)} \\
t_2 &= (ay_c - ay_p) - \frac{F(D - h_1)}{\eta(g - q_1)} \\
t_3 &= (ay_c - ay_p) - \frac{F(D - h_1)}{\eta(g - q_2)}
\end{aligned} \tag{28}$$

The values t_1, t_2, t_3, are taken from the orientation in y-axis, $q_0 = 0$ and the values q_1, q_2, are provided by the electromechanical device. These values are substituted in Eq. (28) and the equation system is solved. Thus, the constants ay_c, ay_p, and ℓ_b are determined. In this manner the camera parameters are calibrated based on the BAN and image processing of the stripe.

The distortion is observed by means of the stripe position ax_p in the image plane, which is described by

$$ax_p = \frac{F\ell_a}{D - h_i} + ax_c \tag{29}$$

Based on Eq. (29), the behavior of ax_p respect to h_i is a linear. However, due to the distortion, the real data ax_p are not linear. The BAN is constructed by means of the real data using the displacement $s_i = (ax_c - ax_p) - (ax_c - ax_o)$. Therefore, the BAN produces a non linear data h, which is shown in Figure 10e. Thus, the distortion is included in the BAN, which computes the object depth in the imaging system.

For a binocular system Figure 2, the object surface z_i is computed via Eq. (3), where $\delta = ax_c - ax_p$ and $\varepsilon = ex_c - ex_p$, respectively. From Eq. (3), the surface z_i depends on the variation the disparity (Mustafa, 2006). Based on the stripe displacement, the disparity is described by $\delta + \varepsilon = as_i + (ax_c - ax_o) + es_i + (ex_c - x_o)$. Thus, the disparity is preserved and the object surface can be computed based on the disparity $\delta + \varepsilon$. In the case of the BAN, the object surface is obtained using only one of two components of the disparity $ax_o - ax_p$ or $ex_o - ex_p$. These two expressions are computed along the laser stripe in the image and processed by the BAN to perform the object contouring. Thus, a transverse section of the object is produced from each stripe image. By means of the information of all stripe images, the complete object is constructed.

VI. EXPERIMENTAL RESULTS

The approach of the Binocular imaging in this technique is to avoid the stripe occlusions. When an occlusion appears, the object contour is not completed. However, in a binocular imaging one of two images provides the occluded stripe and the object contour is completed. Based on the BAN, the parameters of the binocular setup are computed and physical measurements are avoided. Thus, the contouring is performed automatically by computer algorithms. In this manner, the computational performance provides all parameters to

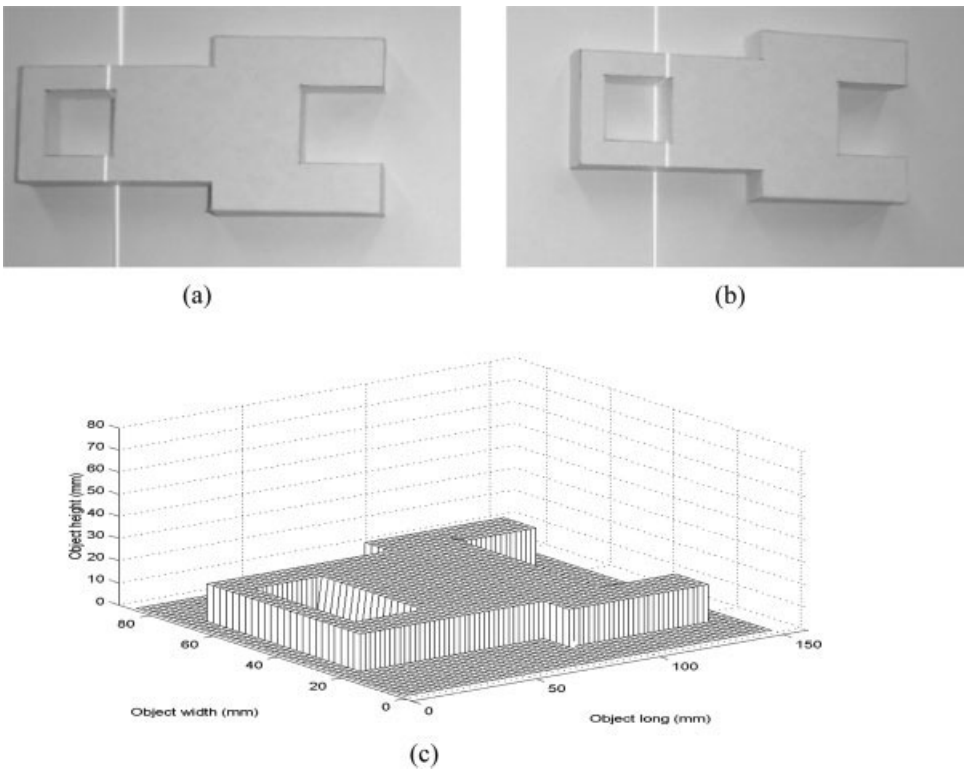

Figure 11. (a) First image of the mechanical piece with stripe occlusion. (b) Second image of the mechanical piece with out stripe occlusion. (c) Three-dimensional shape of the mechanical piece.

reconstruct the object shape. Figure 1 shows the experimental setup. The object is moved in the x-axis by means of the electromechanical device in steps of 1.77 mm. A laser stripe is projected on the target by a 15 mW laser diode to perform the scanning. The stripe is captured by two CCD cameras and digitized by a frame grabber of 256 gray levels. By means of image processing, the displacement as and es are computed. Then, the object dimension $h(x,y)$ is computed via Eq. (15) or Eq. (15). From each pair of the binocular images, a transverse section of the object is produced. The information of all transverse sections is stored in array memory to construct the complete object shape.

The experiment is performed with five objects. The first object to be profiled is a mechanical piece, shown in Figures 11a and 11b. The object surface produces stripe occlusions shown in Figure 11a. In this case, the second image Figure 11b provides the area of the occluded stripe. Therefore, the object reconstruction can be done by means of the binocular imaging. To carry it out, the mechanical piece is scanned in the x-axis in steps of 1.27 mm and binocular images of the stripe are captured. From each pair of images, the first image is used to detect the stripe displacement as. If the first image contains stripe occlusions, the second image will be used to detect the stripe displacement es. The stripe occlusion is detected based pixel of the stripe. If the pixels of high intensity is minor than three in a row, a stripe occlusion is detected in the image. By image processing, the stripe displacement as or es is calculated via Eq. (1) or Eq. (2), respectively. Then, the values u and v are deduced via Eq. (13) and Eq. (14). By means of the BAN Eq. (16) or Eq. (17), the object dimension is computed via u or v, respectively. Thus, the BAN produces a transverse section based on the binocular images. The data produced by the BAN are stored in array memory to construct the complete object shape. To know the accuracy of the data provided by the BAN, the root mean squared error (rms) is calculated (Press et al., 1993) based on a contact method. To carry it out, the object is measured by a coordinate measure machine (CMM). To compute the rms, the data provided by the BAN are compared with respect to the reference data provided by the CMM. The rms is described by the next equation (Masters, 1993)

$$rms = \sqrt{\frac{1}{n}\sum_{i=1}^{n}(ho_i - hc_i)^2}, \tag{30}$$

where ho_i is the data measured by the CMM, hc_i is the calculated data $h(x,y)$ by BAN and n is the number of data. For the mechanical piece, $n = 480$ data to calculate the rms. The error calculated for the mechanical piece is $rms = 0.114$ mm. Sixty-four binocular images were processed to obtain the complete object shape, which is shown in Figure 11c. In this Figure, the scale of the axis is in millimeter.

The second object to be profiled is a dummy face see Figures 12a and 12b. Also, the stripe occlusion that appears in Figures 2a and 12b provides the occluded stripe. To perform the contouring, the dummy face is scanned in x-axis in steps of 1.27 mm. By processing stripe displacements by means of the BAN the shape contour is obtained. In this case, 60–80 stripes were processed to determine the complete object shape shown in Figure 12c. The scale of this figure is millimeter. To determine accuracy of the data provided by the BAN, the dummy face was measured by the CMM. The rms was computed using $n = 1122$ data, which were provided by the BAN and by the CCM as reference. The rms is calculated for this object is rms = 0.155 mm.

The third object to be profiled is a plastic fruit Figure 13a. This image corresponds to the stripe without occlusions. The contouring is performed by scanning the fruit in steps of 1.27 mm. In this case,

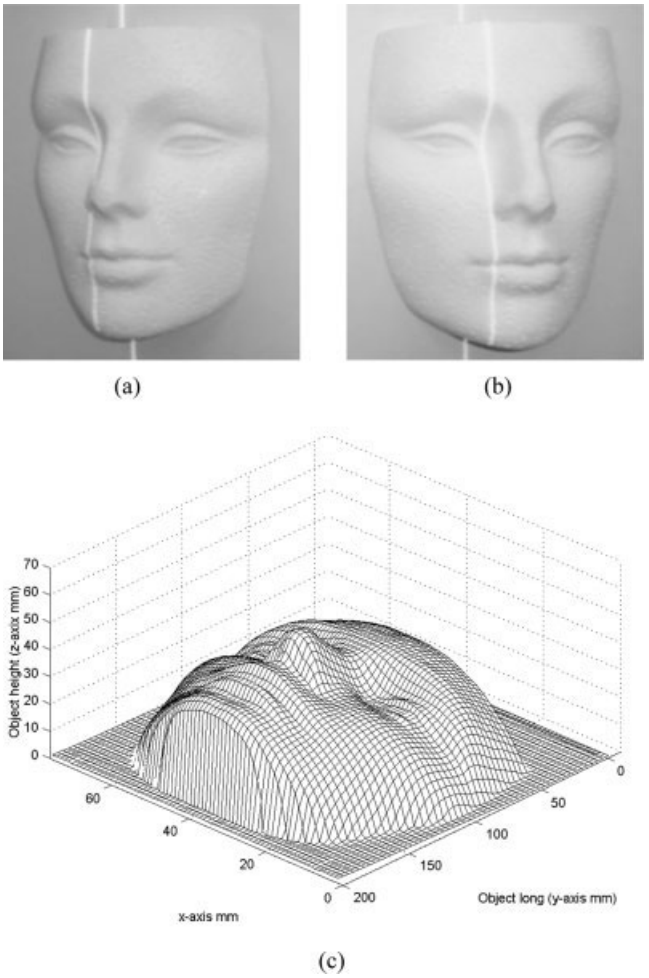

Figure 12. (a) First image of the dummy face with stripe occlusion. (b) Second image of the dummy face with out stripe occlusion. (c) Three-dimensional shape of the dummy face.

46 stripes were processed to determine the complete object shape shown in Figure 13b. To determine accuracy of the data provided by the BAN, the plastic fruit was measured by the CMM. The rms was computed using $n = 420$ data, which were provided by the BAN and by the CMM as reference. The rms is calculated for this object is rms = 0.142 mm.

The fourth object to be profiled is a metallic piece Figure 14a. The contouring is performed by scanning the metallic piece in steps of 1.27 mm. In this case, 58 stripes were processed to determine the complete object shape shown in Figure 14b. The metallic piece was measured by the CMM to determine the accuracy provided by the BAN. The rms was computed using $n = 480$ data, which were provided by the BAN and by the CMM as reference. The rms is calculated for this object is rms = 0.114 mm.

The fifth object profiled is a ceramic glass Figure 15a. This image corresponds to the stripe without occlusions. The contouring is performed by scanning the ceramic glass in steps of 1.27 mm. In this case, 58 stripes were processed to determine the complete object shape shown in Figure 15b. The metallic piece was measured by the CMM to determine the accuracy provided by the BAN. The rms was computed using $n = 520$ data, which were provided by the BAN and by the CMM as reference. The rms is calculated for this object is rms = 0.122 mm.

The powerful of the contouring performed by the BAN is shown in the plastic fruit, the metallic piece and the ceramic glass. These objects do not reflect a uniform intensity of the laser stripe. Therefore, the stripe intensity is not a smooth function Figure 16. In this manner, the stripe detection based on maximum position is not accurate. However, the Bezier curves generate a smooth intensity from the stripe intensity shown in Figure 16. Thus, the stripe detection is accurate and the BAN produces an accurate object contour. This is elucidated by accuracy result of the plastic fruit, the metallic piece and the ceramic glass. In the case of the Gaussian approximation, the accuracy is not better than the accuracy provided by Bezier curves. This is because, the maximum position depend on the pixel number, whose behavior is not Gaussian. Figure 16 shows the Gaussian approximation and its maximum position. The error produced by the Gaussian approximation is rms = 0.122 mm for the mechanical piece, for the dummy face the is rms = 0.168 mm, for the plastic fruit is rms = 0.157 mm, for the metallic piece is rms = 0.126 mm and for the ceramic glass is rms = 0.134 mm. These results indicates that the stripe detection by Bezier curves provide better contouring accuracy than Gaussian approximation. Therefore, the BAN used Bezier curves to detect the stripe position to perform the object contouring. Also, contouring performed by the BAN and binocular imaging provides better accuracy than similar techniques implemented in the last years. For comparison, the error of these techniques is mentioned as follow. Profiling with stereo matching and occlusions, the reported error is over 8% (Luo et al.;

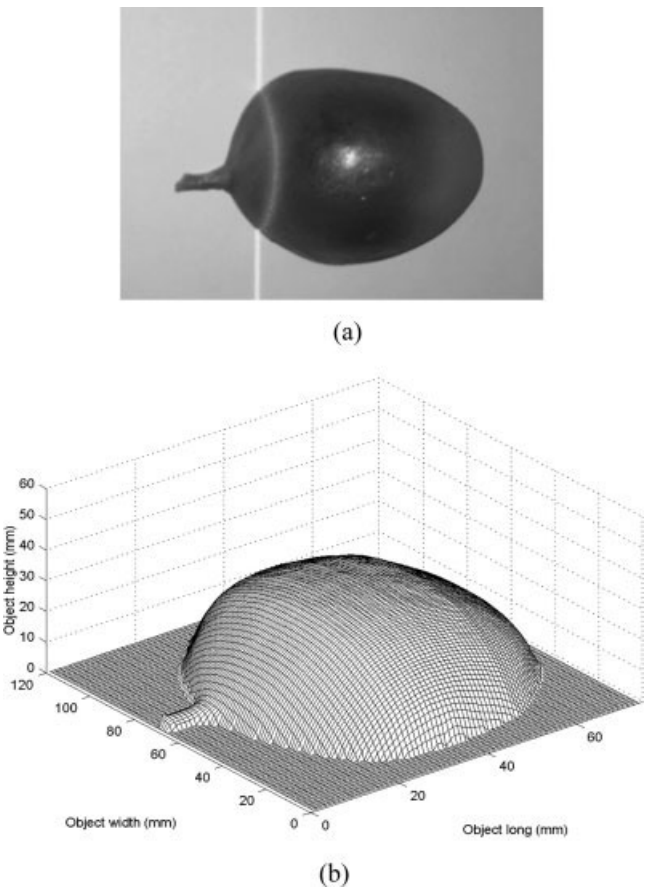

Figure 13. (a) Image of the plastic fruit with out stripe occlusion. (b) Three-dimensional shape of the plastic fruit.

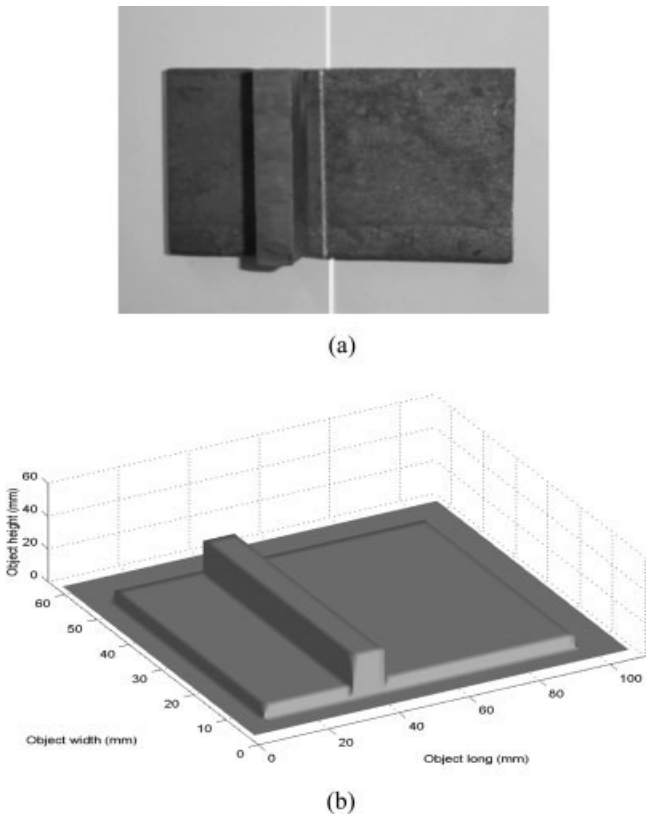

Figure 14. (a) Image of the metallic piece with out stripe occlusion. (b) Three-dimensional shape of the metallic piece.

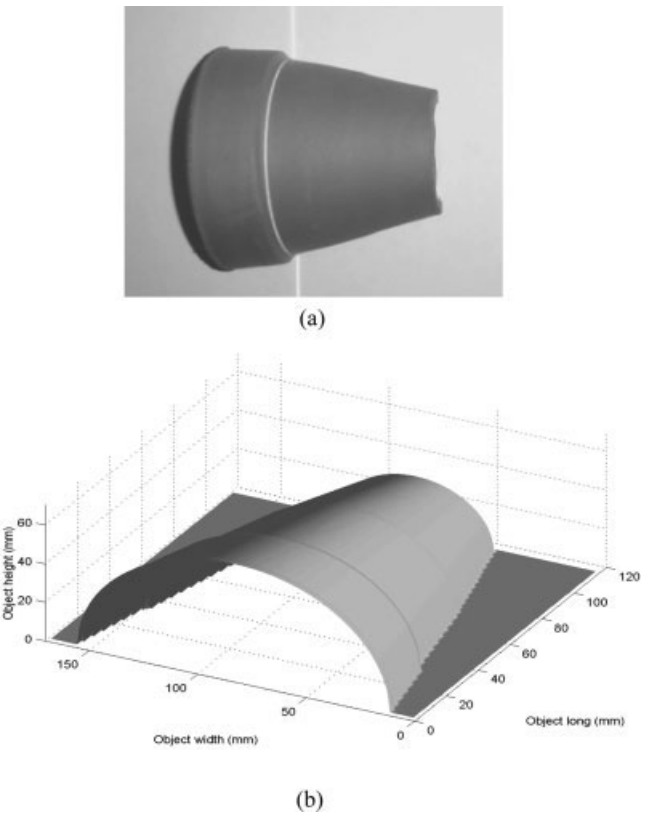

Figure 15. (a) Image of the ceramic glass with out stripe occlusion. (b) Three-dimensional shape of the ceramic glass.

2003). A technique for face profiling based on stereo reports an error over 1% (Hong-Liu and Mustafa, 2006). A technique correlation-based stereo matching reports an error over 2.3 % (Sukjune and Sun-Kee, 2005). A welding system based on stereo vision reports an error of 1.68 mm (Pi-Chen et al., 2004). A 3D surface measurement based on structured light and stereo vision reports an error of an rms = 0.4074 (Junhua et al., 2006). These results indicate that the BAN and Bezier stripe detection of binocular imaging provide better accuracy in the object contouring. The error provide by the BAN is minor then 1%.

The value n has an influence in the confidence level respect to the precision of the error calculated. To determine if the value n is according to the desired precision, the confidence level is calculated by the next relation (Freund, 1979)

$$n = \left(z_\alpha \frac{\sigma_x}{e}\right)^2 \tag{31}$$

where z_α is the confidence desired, e is the error expressed in percentage, and σ_x is standard deviation. Therefore, the confidence level according to the data n can be described by

$$z_\alpha = \frac{e}{\sigma_x}\sqrt{n}. \tag{32}$$

To know if the value n chosen is according with the confidence of level desired Eq. (31) is applied. The confidence level desired is 95 %, which corresponds to $z_\alpha = 1.96$ according to the confidence table (Freund, 1979). The average of the height of the face surface is 19.50 mm, therefore using the rms the error is 0.0079, which represents a 0.79 % of error. To determine the precision of this error, the confidence level is calculated for the $n = 1122$, $e = 0.79$ and standard deviation is 7.14. Substituting the values in Eq. (32), the result is $z_\alpha = 3.7061$. It indicates a confidence level greater than the 95%. Also, the confidence level is greater than 95% for the mechanical piece, the plastic fruit, the metallic piece and the ceramic glass.

The employed computer in this process is a PC to 1 GHz. Each stripe image is processed in 0.011 s. This time processing is given because the data of the image is extracted with few operations via Eq. (4). The capture velocity of the camera used in this camera is 34 fps. The electromechanical device is moved also at 34 steps per

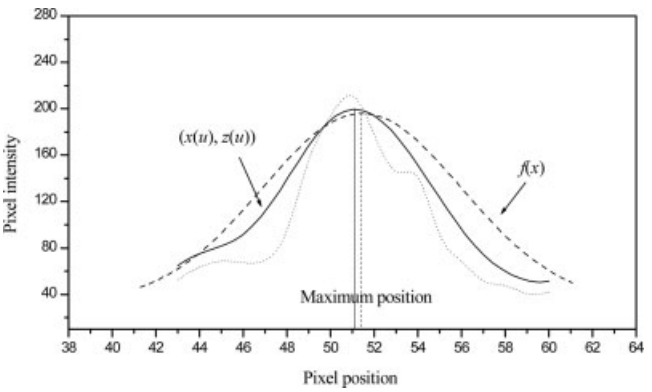

Figure 16. Bezier curves and Gaussian approximation of a not smooth stripe.

second. The complete shape of the mechanical piece profiled in 2.91 s, the dummy face is profiled in 4.18 s, the plastic fruit face is profiled in 2.58 s, the metallic piece is profiled in 3.22 s, the ceramic glass is profiled in 3.68 s. In this procedure, distances of the geometry of the setup to obtain the object shape are not used. Therefore, the procedure is easier than those techniques that use distances of the components of optical setup. In this manner, the technique is performed by computational process and measurements on optical step are avoided. Therefore, a good repeatability achieved in experiment of a standard deviation +/− 0.01 mm. In the case of deep valley, the distance between two cameras should be reduced. The observation of the deep surface depends on the distance between the cameras. For our binocular system the deep surface about 200 mm can observed.

VII. CONCLUSIONS

A technique for shape detection performed by means of tripe projection, binocular imaging and approximation networks has been presented. The described technique here provides a valuable tool for inspection industrial and reverse engineering. The automatic technique avoids the physical measurements of the setup, as is common in the methods of laser stripe projection. In this technique, the parameters of the setup are obtained automatically by computational process using BAN. It improves the accuracy of the results, because measurement errors are not introduced to the system for the shape detection. In this technique, the ability to measure the stripe behavior with a sub-pixel resolution has been achieved by Bezier curves. It is achieved with few operations. By using this computational-optical setup a good repeatability is achieved in every measurement. Therefore, this technique is performed in good manner.

ACKNOWLEDGMENTS

J. Apolinar Muñoz Rodríguez would like to thank CONCYTEG of Guanajuato and CONACYT Mexico for the partial support of this research.

REFERENCES

Y.J. Ahn, Y.S. Kim, and Y. Shin, Approximation of circular arcs and o set curves by Bezier curves of high degree, J Comp Appl Math 167 (2004), 405–416.

H.J. Andersen, L. Reng, and K. Kirk, Geometric plant properties by relaxed stereo vision using simulated annealing, Comput Electron Agric 49 (2005), 219–232.

M. Baba, T. Konishi, and N. Kobayashi, A novel fast rangefinder with non-mechanical operation, J Opt 29 (1998), 241–249.

F. Causa and J. Sarma, Realistic model for the output beam profile of stripe and tapered superluminescent light-emitting diodes, Appl Opt 42 (2003), 4341–4348.

G.D. Chen and G.J. Wang, Optimal multi-degree reduction of Bézier curves with constraints of endpoints continuity, Comput Aided Geometric Des 19 (2002), 365–377.

H. Frederick and G.J. Lieberman, Introduction to operations research, McGraw-Hill, USA, 1982.

J.E. Freund, Modern elementary statistics, Prentice Hall, USA, 1979.

P.C. Gasson, Geometry of spatial forms, Wiley, USA, 1989.

C.F. Gerald and P.O. Wheatley, Applied numerical analysis, Addison Wesley, USA, 1992.

C. Hong-Liu and J. Ward Mustafa, The use of 3D information in face recognition, Vision Res 46 (2006), 768–773.

S. Junhua, Z. Guangjun, W. Zhenzhong, and Z. Fuqiang, Large 3D free surface measurement using a mobile coded light-based stereo vision system, Sens Actuators A: Phys 132 (2006), 460–471.

R. Klette, K. Schluns, and A. Koschan, Computer vision: Three-dimensional data from images, Springer, Singapore, 1998.

T. Masters, Practical neural networks recipes in C++, Academic Press, USA, 1993.

Q. Luo, J. Zhou, S. Yu, and D. Xiao, Stereo matching and occlusion detection with integrity and illusion sensitivity, Pattern Recognit Lett 24 (2003), 1143–1149.

A.M. Mclvor, Nonlinear calibration of a laser profiler, Opt Eng 42 (2002), 205–212.

J.S. Milton and J.C. Arnold, Introduction to probability and statistics: Principles and applications for engineering and the computing science, McGraw-Hill, USA, 2003.

H. Mitsudo, S. Nakamizo, and H. Ono, A long-distance stereoscopic detector for partially occluding surfaces, Vision Res 46 (2006), 1180–1186.

J.A. Muñoz Rodríguez and R. Rodríguez-Vera, Evaluation of the light line displacement location for object shape detection, J Mod Opt 50 (2003), 137–154.

G. Mustafa, Neural network analysis of head-flow curves in deep well pumps, Energy Conversion Manage 47 (2006), 992–1003.

T. Pi-Chen, W. Ming-Chang, and H. Yean-Ren, An image-guided mobile robotic welding system for SMAW repair processes, Vision Res Int J Machine Tools Manufacture 44 (2004), 1223–1233.

W.H. Press, B.P. Flannery, S.A. Teukolsky, and W.T. Vetterling, Numerical recipes in C, Cambridge Press, USA, 1993.

R.J. Schalkoff, Artificial neural networks, McGraw Hill, USA, 1997.

Y. Sukjune and P. Sun-Kee, Fast correlation-based stereo matching with the reduction of systematic errors, Pattern Recognit Lett 26 (2005), 2221–2231.

W. Ch. Tai and M. Chang, Non contact profilometric measurement of large form parts, Opt Eng 35 (1996), 2730–2735.

Z. Wei, G. Zhang, and Y. Xu, Calibration approach for structured-light-stripe vision sensor based on invariance of double cross-ratio, Opt Eng 42 (2003), 2956–2966.

L. Zagorchev and A. Goshtasby, A paintbrush laser range scanner, Comput Vision Image Understating 10 (2006), 65–86.